Multiplicity Features of Nonadiabatic, Autothermal Tubular Reactors

Marianne Lovo and Vemuri Balakotaiah
Dept. of Chemical Engineering, University of Houston, Houston, TX 77204

Singularity theory is combined with asymptotic analysis to determine the exact uniqueness-multiplicity boundary and ignition and extinction locus for the nonadiabatic, autothermal tubular reactor model. It is found that the steady-state behavior of the nonadiabatic reactor is described by the two limiting cases of adiabatic and strongly cooled models. The adiabatic case has been examined in a previous study. Here, we develop limiting models to describe the strongly cooled asymptotes. We also classify the different types of bifurcation diagrams of conversion vs. residence time using the results of singularity theory with a distinguished parameter. Analytical criteria are developed for predicting the conditions under which autothermal operation is feasible when heat losses are significant.

Introduction

Tubular reactors with internal heat exchange are part of a class of reactors that operate autothermally. These autothermal processes involve a feedback of heat that leads to the presence of multiple steady states. This is important in the operation of autothermal tubular reactors since these reactors usually operate on the upper ignited steady state. Many theoretical and experimental studies have examined this behavior for autothermal tubular reactors (van Heerden, 1953; Baddour et al., 1965; Inoue and Komiya, 1969; Ampaya and Rinker, 1977). In a previous work (Lovo and Balakotaiah, 1991), we analyzed the multiplicity features of the adiabatic autothermal tubular reactor.

In many instances, these reactors operate nonadiabatically. One case of particular importance is the deep-well oxidation reactor which is used to oxidize dilute aqueous waste streams (Lovo et al., 1990). This reactor shown in Figure 1, consists of concentric tubes, 1,500-3,000 m long, suspended within a conventionally drilled and cased well. The waste enters the reactor at the surface and flows down the center tube. Oxygen is pumped through an inner tube and is introduced at the bottom of the reactor where temperatures (250-350°C) and pressures are high (10-20 MPa). Organic oxidation is spontaneously initiated at these conditions, and the reaction occurs in a very small section at the bottom of the reactor. The oxidation products, carbon dioxide and water, then flow up through the outer annulus and leave the reactor at the surface. In many respects, this reactor is similar to the conventional autothermal reactors; however, there is one major difference. The reactor operates nonadiabatically and may lose a significant amount of the heat generated to the surrounding earth. The goal of this work is to examine the steady-state behavior of such nonadiabatic, autothermal tubular reactors.

The nonadiabatic case of the autothermal tubular reactor has been examined by a few authors in a more limited context than the adiabatic case. Ampaya and Rinker (1977) investigated the behavior of autothermal reactors both experimentally and numerically. A one-dimensional adiabatic model and a two-dimensional nonadiabatic model were considered. Although heat losses were examined, the main goal of the study was to verify experimentally multiple steady states in an autothermal reactor with internal heat exchange and to compare the experimental results with those obtained numerically and to examine the effect of radial gradients within the reactor. Adomaitis and Cinar (1988) considered the nonadiabatic, autothermal reactor with both heat and mass dispersion and examined the bifurcation behavior of the reactor with the dimensionless flow rate as the bifurcation variable for various values of inlet temperature and concentration. They used the collocation method to discretize the equations and some analogies to singularity theory to classify the different types of bifurcation behavior. These previous studies did not address the important issue of determining the region of autothermal operation for the nonadiabatic case.

In this work, we examine the multiplicity features of the nonadiabatic, autothermal tubular reactor. We use the singularity theory and combine it with the asymptotic analysis to

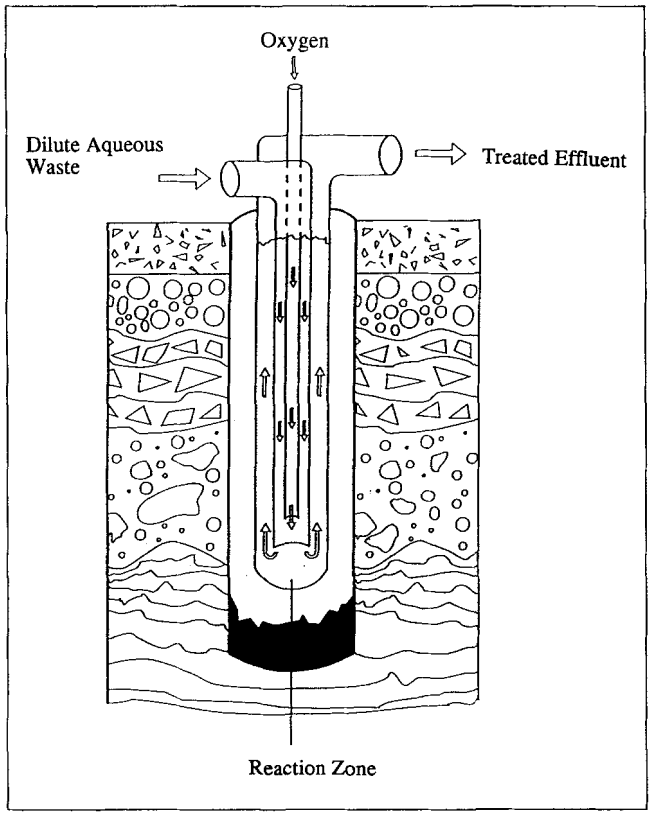

Figure 1. Deep-well oxidation reactor.

determine the exact uniqueness-multiplicity boundary and cross-sections of the bifurcation set (ignition and extinction locus) for the nonadiabatic, autothermal tubular reactor model. We also classify the different types of bifurcation diagrams of conversion vs. residence time using the results of singularity theory with a distinguished parameter. Finally, we develop analytical criteria for predicting the conditions under which autothermal operation is possible for the nonadiabatic tubular reactor with internal countercurrent heat exchange.

Mathematical Treatment

We consider an autothermal reactor in which a first-order, irreversible, exothermic reaction $A \rightarrow B$ occurs. We assume that heat and mass dispersion effects are negligible. The downtube (inner or preheating tube) of the reactor is used as the preheat zone, and the reaction occurs in the uptube (outer reaction tube) of the reactor. We assume that the temperature of the feed is the same as that of the coolant or surroundings. The resulting steady-state model is given by:

$$\frac{dy_d}{d\xi} = -St\ (y_d - y_u) \tag{1}$$

$$\frac{dy_u}{d\xi} = -\beta\ Da\ (1-\chi)\ \exp\ \{\gamma\ y_u/(1+y_u)\} - St\ (y_d - y_u) + \alpha\ y_u \tag{2}$$

$$\frac{d\chi}{d\xi} = -Da\ (1-\chi)\ \exp\ \{\gamma\ y_u/(1+y_u)\} \tag{3}$$

with boundary conditions

$$\chi(\xi=1)=0;\ y_d\ (\xi=1)=y_u(\xi=1);\ y_d(\xi=0)=0. \tag{4}$$

The dimensionless groups that appear in Eqs. 1-3 are defined previously (Lovo and Balakotaiah, 1991). This model contains one additional parameter α, which is a measure of the heat transfer between the outer tube and the surroundings, and is defined as:

$$\alpha = \frac{A_{hu} U_u}{q\ \rho_f\ C_{pf}}. \tag{5}$$

The two energy balance equations (Eqs. 1-2) may be combined to eliminate y_u. The resulting equations for y_d and χ follow. For convenience, we drop the subscript for the downtube and refer to y_d as y:

$$\frac{d^2y}{d\xi^2} - \alpha\ \frac{dy}{d\xi} - \alpha\ St\ y + \beta\ St\ Da\ (1-\chi)\ \exp\left\{\frac{\gamma\left(y + \frac{1}{St}\frac{dy}{d\xi}\right)}{1 + y + \frac{1}{St}\frac{dy}{d\xi}}\right\} = 0 \tag{6}$$

$$\frac{d\chi}{d\xi} + Da\ (1-\chi)\ \exp\left\{\frac{\gamma\left(y + \frac{1}{St}\frac{dy}{d\xi}\right)}{1 + y + \frac{1}{St}\frac{dy}{d\xi}}\right\} = 0 \tag{7}$$

$$\chi(\xi=1)=0;\ y(\xi=0)=0;\ \frac{dy}{d\xi}(\xi=1)=0. \tag{8}$$

We analyze the problem in the same manner as the adiabatic case (Witmer et al., 1986; Lovo and Balakotaiah, 1991).

Determination of Uniqueness-Multiplicity Boundary

We determine the uniqueness-multiplicity boundary for the nonadiabatic reactor by fixing the ratio of the heat transfer to the surroundings (α) to the heat transfer between the up- and downtubes (St). Typical ratios are small ($\alpha/St \ll 1$). In Figure 2, we show the numerically computed cusp locus in the $\gamma - \beta$ plane for a fixed ratio of heat transfer to heat losses ($\alpha/St = 0.01$). For small values of St, $St = 0.1$ and $St = 1$, we observe that the cusp locus remains very close to that of the adiabatic case. For larger values of St, however, we observe that the uniqueness-multiplicity boundary shifts to the right of the adiabatic values. Therefore, for a fixed activation energy, γ, the nonadiabatic reactor requires larger values of β or higher inlet concentrations than the adiabatic rector to achieve an ignited state. Although this result is intuitive, we note that at high values of the Stanton number (St = 10, 100) the cusp curves become compressed into essentially a single curve, and increasing the Stanton number (with α/St fixed) has no effect on the range of (γ, β) values for which multiple solutions are possible.

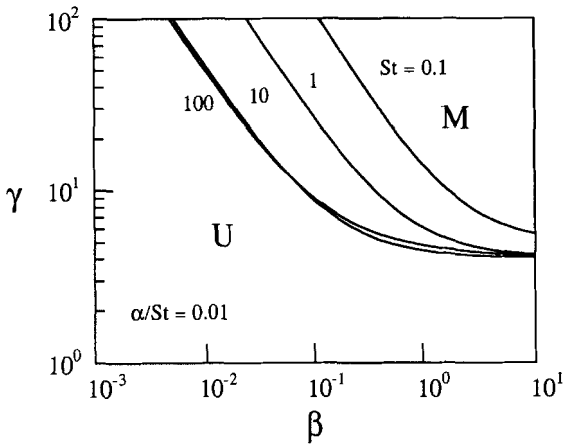

Figure 2. Exact uniqueness-multiplicity boundary in the (γ, β) space for different Stanton numbers.

U and *M* denote regions of multiplicity and uniqueness.

The calculations in Figure 2 show that three limiting models exist. The first two limiting models describe the two distinct asymptotes which are observed for $\beta \ll 1$ and $\beta \gg 1$. The third limiting model describes the case when heat transfer is high and the uniqueness-multiplicity curves become compressed into a single curve. We now describe each of these asymptotes by the appropriate limiting models below.

Positive exponential approximation model ($\beta \ll 1$, $\gamma \gg 1$, $\gamma\beta$ = finite)

For the case of small β, we assume that the temperature $y_u(1)$ is small compared to unity so that the positive exponential approximation may be used. Defining

$$\theta = \gamma y \quad B = \gamma\beta, \tag{9}$$

the limiting model is given by:

$$\frac{d^2\theta}{d\xi^2} - \alpha \frac{d\theta}{d\xi} - \alpha \, \mathrm{St} \, \theta + B \, St \, Da \, (1-\chi) \exp\left\{\theta + \frac{1}{St}\frac{d\theta}{d\xi}\right\} = 0 \tag{10}$$

$$\frac{d\chi}{d\xi} + Da \, (1-\chi) \exp\left\{\theta + \frac{1}{St}\frac{d\theta}{d\xi}\right\} = 0 = 0 \tag{11}$$

$$\chi(\xi = 1) = 0; \; \theta(\xi = 0) = 0; \; \frac{d\theta}{d\xi}(\xi = 1) = 0. \tag{12}$$

This model contains four parameters: α, St, Da, and B. We can reduce the number of parameters further by analyzing only the case of most practical interest (large St and small α). This allows us to drop the terms containing $d\theta/d\xi$ in Eqs. 10 and 11. The resulting model has three parameters, $B^* = B\,St$, Da, and αSt and is given as:

$$\frac{d^2\theta}{d\xi^2} - \alpha \, St \, \theta + B^* Da \, (1-\chi) \exp\{\theta\} = 0 \tag{13}$$

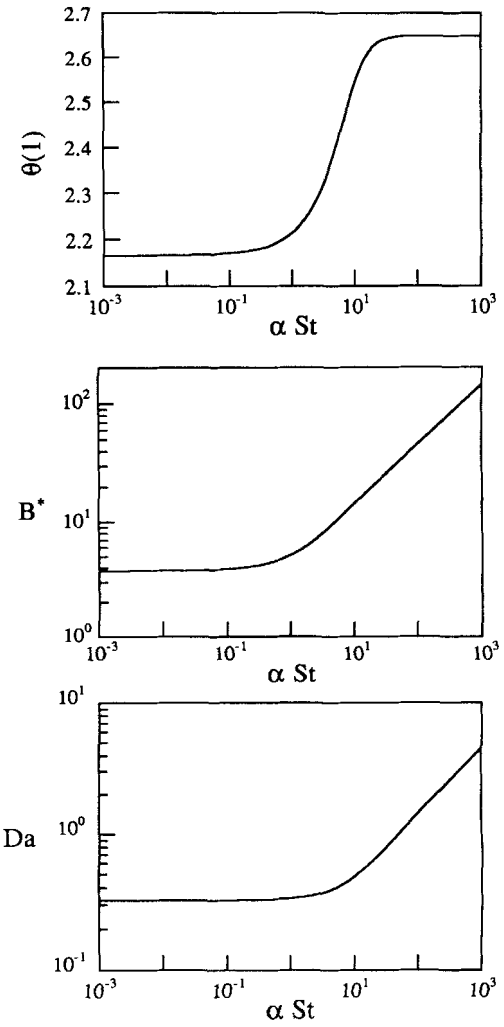

Figure 3. Dependence of $\theta(1)$, B^*, and Da at the cusp point on αSt for the positive exponential approximation model.

$$\frac{d\chi}{d\xi} + Da \, (1-\chi) \exp\{\theta\} = 0 \tag{14}$$

$$\chi(\xi = 1) = 0; \; \theta(\xi = 0) = 0; \; \frac{d\theta}{d\xi}(\xi = 1) = 0. \tag{15}$$

Figure 3 shows the locus of cusp points for this simplified PEA (positive exponential approximation) model [$\beta \ll 1$ and $(\alpha/St) \ll 1$]. For each value of αSt, we can find the cusp coordinates in terms of $\theta(1)$, B^* and Da. By treating the problem in this manner, we can clearly identify two limiting cases for small and large values of αSt. The limit of low αSt corresponds to the adiabatic high heat transfer limit where the cusp locus is given by (Lovo and Balakotaiah, 1991):

$$\theta(1) = 2.165; \; B^* = 3.777; \; Da = 0.3223. \tag{16}$$

The limit of large αSt corresponds to the strongly cooled case where the cusp locus is given by:

$$\theta(1) = 2.649$$

$$\frac{B^*}{\sqrt{\alpha\, St}} = 4.549 \tag{17}$$

$$\frac{Da}{\sqrt{\alpha\, St}} = 0.1432.$$

Negligible reactant consumption model ($\beta >> 1$, $\beta >> Da$)

For the case of $\beta \gg 1$, we may neglect reactant consumption. This results in the following limiting model:

$$\frac{d^2y}{d\xi^2} - \alpha \frac{dy}{d\xi} - \alpha\, St\, y + \delta \exp\left\{\frac{\gamma\left(y + \frac{1}{St}\frac{dy}{d\xi}\right)}{1 + y + \frac{1}{St}\frac{dy}{d\xi}}\right\} = 0 \tag{18}$$

$$y(\xi = 0) = 0;\ \frac{dy}{d\xi}(\xi = 1) = 0, \tag{19}$$

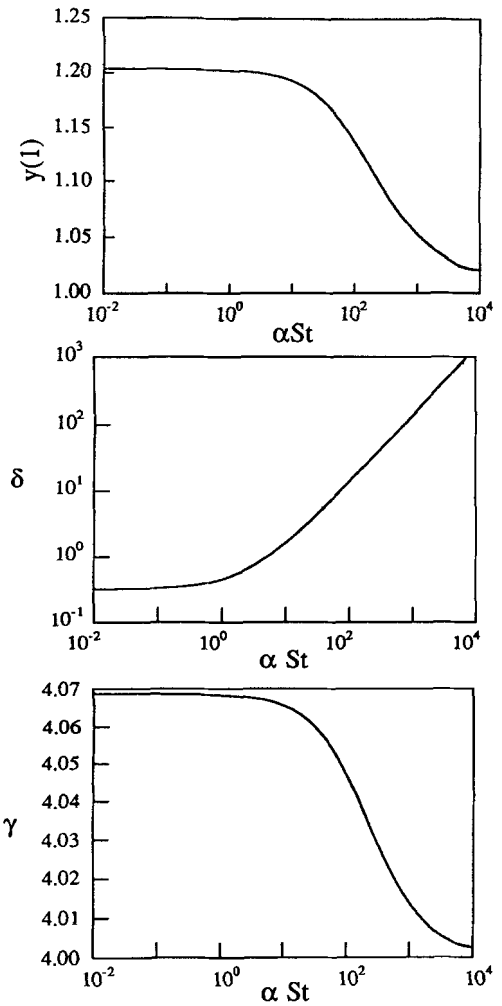

Figure 4. Dependence of $y(1)$, δ and γ at the cusp point on αSt for the negligible reactant consumption model.

where

$$\delta = \beta\, St\, Da. \tag{20}$$

This model is described by four parameters, γ, δ, α, and St. Again, we may reduce the number of parameters by considering only the case of $St \gg 1$ and $\alpha \ll St$. The simplified model is given by:

$$\frac{d^2y}{d\xi^2} - \alpha\, St\, y + \delta \exp\left\{\frac{\gamma y}{1+y}\right\} = 0 \tag{21}$$

$$y(\xi = 0) = 0;\ \frac{dy}{d\xi}(\xi = 1) = 0. \tag{22}$$

Figure 4 shows the cusp locus as a function of αSt for this simplified model [$\beta \gg 1$, $\alpha/St << 1$]. Again, we observe the adiabatic and strongly cooled limits. In the limit of small αSt, the cusp locus approaches the adiabatic asymptote of (Lovo and Balakotaiah, 1991):

$$y(1) = 1.203;\ \gamma = 4.068;\ \delta = 0.3213. \tag{23}$$

The limit of large αSt corresponds to the strongly cooled case where the cusp locus is given by:

$$y(1) = 1.000$$

$$\gamma = 4.000 \tag{24}$$

$$\frac{\delta}{\alpha St} = e^{-2} = 0.1353.$$

Strongly cooled model [$\alpha\, St >> 1$, (α/St) = finite]

We now develop a limiting model for the strongly cooled case. For the strongly cooled limit of the positive exponential approximation model, we observed that B^* and Da at the cusp point are proportional to $\sqrt{\alpha St}$. The strongly cooled limit of the negligible reactant consumption model also showed that the cusp point becomes independent of the Damkohler number, and the ratio $(\delta/\alpha St)$ becomes a constant (Da is also proportional to $\sqrt{\alpha St}$). In developing a limiting model to describe this strongly cooled case, we introduce a new dimensionless coordinate to rescale the model described by Eqs. 6-8. For convenience, we also reverse the ξ coordinate. We let

$$\eta = \sqrt{\alpha St}(1 - \xi). \tag{25}$$

The resulting model is:

$$\frac{d^2y}{d\eta^2} + \sqrt{\frac{\alpha}{St}}\frac{dy}{d\eta} - y + \frac{\beta\, Da}{\alpha} \exp\left\{\frac{\gamma\left(y - \sqrt{\frac{\alpha}{St}}\, y'\right)}{\left(1 + y - \sqrt{\frac{\alpha}{St}}\, y'\right)}\right\}(1 - \chi) = 0 \tag{26}$$

$$\frac{d\chi}{d\eta}-\frac{Da}{\sqrt{\alpha\, St}}\exp\left\{\frac{\gamma\left(y-\sqrt{\frac{\alpha}{St}}\,y'\right)}{\left(1+y-\sqrt{\frac{\alpha}{St}}\,y'\right)}\right\}(1-\chi)=0 \tag{27}$$

$$\begin{aligned}\chi(0)&=0\\ y'(0)&=0\\ y(\infty)&=0.\end{aligned} \tag{28}$$

If we make the same assumption as in the simplified models above ($\alpha/St \ll 1$), we may again neglect the terms containing y' to obtain the following simplified model:

$$\frac{d^2y}{d\eta^2}-y+\frac{\beta\, Da}{\alpha}\exp\left\{\frac{\gamma y}{1+y}\right\}(1-\chi)=0 \tag{29}$$

$$\frac{d\chi}{d\eta}-\frac{Da}{\sqrt{\alpha\, St}}\exp\left\{\frac{\gamma y}{1+y}\right\}(1-\chi)=0 \tag{30}$$

$$\begin{aligned}\chi(0)&=0\\ y'(0)&=0\\ y(\infty)&=0.\end{aligned} \tag{31}$$

This model is described by three parameters: γ, $(\beta Da/\alpha)$, and $(Da/\sqrt{\alpha\, St})$. For this model, we may also examine the limiting cases of $\beta>>1$ and $\beta<<1$. These limits correspond to the strongly cooled asymptote ($\alpha St>>1$) of the two previous models.

The case of practical importance for autothermal reactors is the low β asymptote or the strongly cooled limit of the simplified PEA model. This is true particularly for the case of the deep-well reactor where we are interested in dilute aqueous waste streams (large γ and small β). In this case, we can simplify the above model further by making the positive exponential approximation:

$$\frac{d^2\theta}{d\eta^2}-\theta+\frac{\gamma\beta Da}{\alpha}\exp\{\theta\}(1-\chi)=0 \tag{32}$$

$$\frac{d\chi}{d\eta}-\frac{Da}{\sqrt{\alpha\, St}}\exp\{\theta\}(1-\chi)=0 \tag{33}$$

$$\begin{aligned}\chi(0)&=0\\ \theta'(0)&=0\\ \theta(\infty)&=0.\end{aligned} \tag{34}$$

This model has only two parameters and a single cusp point given by Eq. 17.

We may also consider the limiting case of negligible reactant consumption. In this case, the model also has only two parameters and is described by:

$$\frac{d^2y}{d\eta^2}-y+\frac{\beta Da}{\alpha}\exp\left\{\frac{\gamma y}{1+y}\right\}=0 \tag{35}$$

$$\begin{aligned}y'(0)&=0\\ y(\infty)&=0.\end{aligned} \tag{36}$$

This model has a single cusp point given by Eq. 24.

Results with residence time as bifurcation variable

The steady-state behavior of the nonadiabatic, autothermal reactor can be better understood by looking at the different types of bifurcation diagrams that describe the state variable (bottom temperature) as a function of the residence time. To classify the different types of bifurcation diagrams of temperature (or conversion) vs. residence time, we rewrite the steady state equations (Eqs. 1-4) such that the residence time occurs only in the Damkohler number. We define $St = H_d\, Da$ and $\alpha = H_u\, Da$, where H_d and H_u are the dimensionless heat transfer coefficients for the downtube and uptube, respectively.

$$\begin{aligned}H_d&=\frac{U_d A_{hd}}{\rho_f C_{pf} k(T_0)\, V_r}\\ H_u&=\frac{U_u A_{hu}}{\rho_f C_{pf} k(T_0)\, V_r}.\end{aligned} \tag{37}$$

The different types of bifurcation diagrams that occur can be classified by utilizing singularity theory with a distinguished parameter (Golubitsky and Schaeffer, 1985; Balakotaiah and Luss, 1984). A change in the type of bifurcation diagram can occur only if the parameters cross one of a number of hypersurfaces in the parameter space. For the adiabatic case, only two different types of bifurcation diagrams (single-valued and S-shaped) were shown to exist for either the Stanton or the residence time formulation (Lovo and Balakotaiah, 1991). The hypersurface that separates the regions of the parameter space where these two different types of bifurcation diagrams of temperature vs. residence time occur is the hysteresis variety.

We examine the effects of reparametrization for the nonadiabatic case by considering the results from the positive exponential approximation model. We note that most cases of practical interest, where γ is large and β is small, are described by this asymptote. Figure 5 shows the reparametrized results of the PEA model such that the residence time occurs only in the Damkohler number. We note that as long as the product of the heat transfer coefficients ($H_d\, H_u$) is small, there exists a hysteresis (cusp) point in this formulation. However, when the product H_dH_u becomes large, the strongly cooled limit is reached and the cusp point moves to $Da = \infty$. This point is defined by the cusp point of the simplified strongly cooled model (Eq. 17). Beyond this point the boundary between different types of bifurcation diagrams is defined by the existence of a limit-point at $Da=\infty$. This is called the boundary limit variety and is defined by the limit points of the strongly cooled model rewritten in the residence time formulation. If we substitute $\alpha = H_u\, Da$ and $St = H_d\, Da$ into Eqs. 26-28 or Eqs. 29-31, the model becomes independent of the Damkohler number or residence time. The strongly cooled model is now defined by the limit of $Da \to \infty$, which is implicit in the boundary condition at infinity. We refer to the two branches of this locus as ignition point at infinity and extinction point at infinity.

Figure 6 shows a cross-section of the hysteresis and boundary

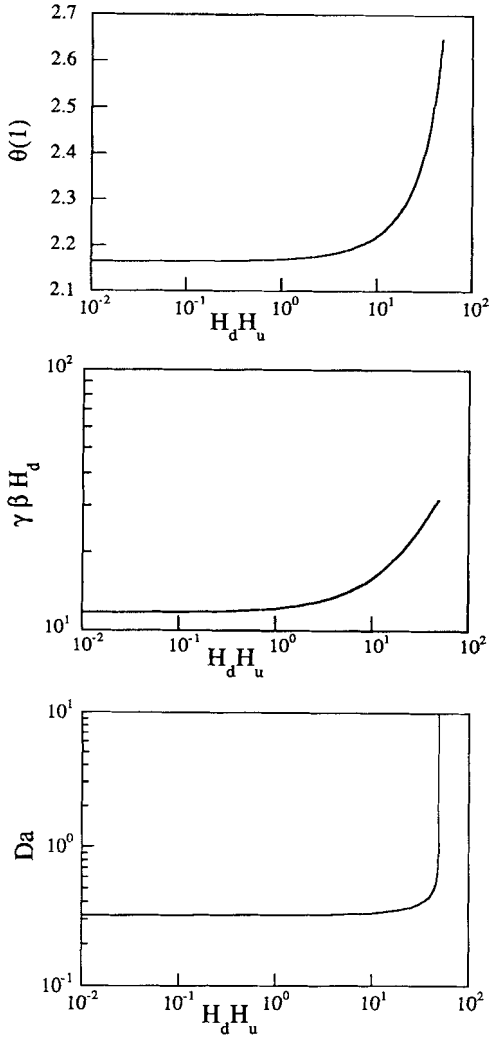

Figure 5. Dependence of $\theta(1)$, $\gamma\beta H_d$ and Da at the cusp point on H_dH_u for the positive exponential approximation model.

limit varieties in the (H_d, H_u) plane for typical values of γ and β. The parameter space is divided into three regions (I-III) where different types of bifurcation diagrams occur. Figures 7, 8 and 9 show the different bifurcation diagrams that occur in the three regions marked on Figure 6. The transitions between these different types of diagrams are characterized by either appearance or disappearance of a hysteresis or the appearance or disappearance of an ignition point or extinction point at $Da = \infty$. We note that for small values of H_u, which corresponds to the pseudo-adiabatic case, only the two behaviors, which were observed for the adiabatic case, exist. In this case, the hysteresis variety may be approximated by the criterion that was previously developed for the adiabatic case ($\gamma\beta H_d = 11.72$).

We note that typical values of H_d are large ($H_d = 10^5 - 10^8$). For these values, we observe all three types of behavior depending on the value of H_u or the magnitude of the heat losses. For small values of H_u, the reactor behavior is pseudo-adiabatic and is characterized by a S-shaped bifurcation diagram with both an ignition and extinction point (type I behavior) shown in Figure 7. When the heat losses are increased to some critical

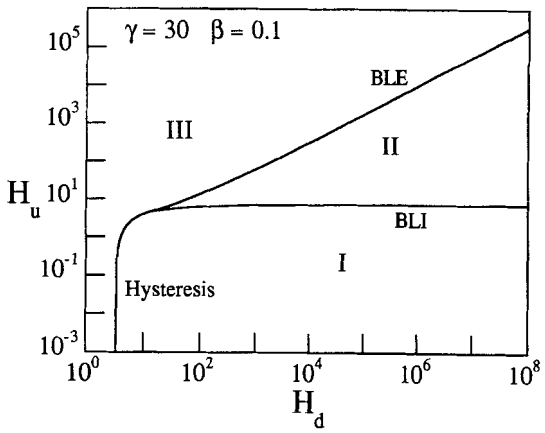

Figure 6. Cross-section of the hysteresis and boundary limit varieties in $H_d - H_u$ plane for $\gamma = 30$, $\beta = 0.1$.

value, described by the boundary limit ignition (BLI), the ignition locus levels off and the ignition point moves to $Da \rightarrow \infty$. Above this, we observe a region where the upper ignited branch is isolated (type II behavior) as shown by the bifurcation diagram of Figure 8. Then, at another critical value of H_u, described by the boundary limit extinction (BLE), the extinction points moves to $Da \rightarrow \infty$. Above this critical value of H_u, we have single-valued bifurcation diagrams of conversion vs. residence time (type III behavior). This type of bifurcation diagram is shown in Figure 9.

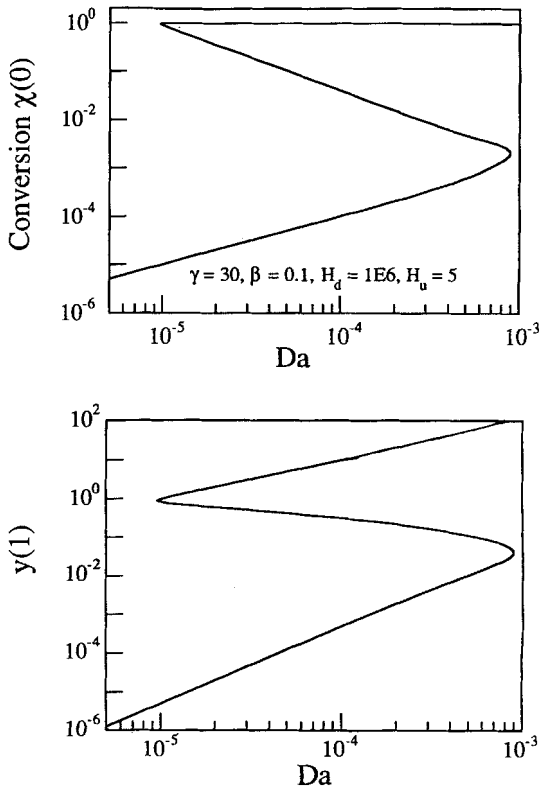

Figure 7. Bifurcation diagrams of bottom temperature and exit conversion vs. Da (residence time) for parameter values in region I.

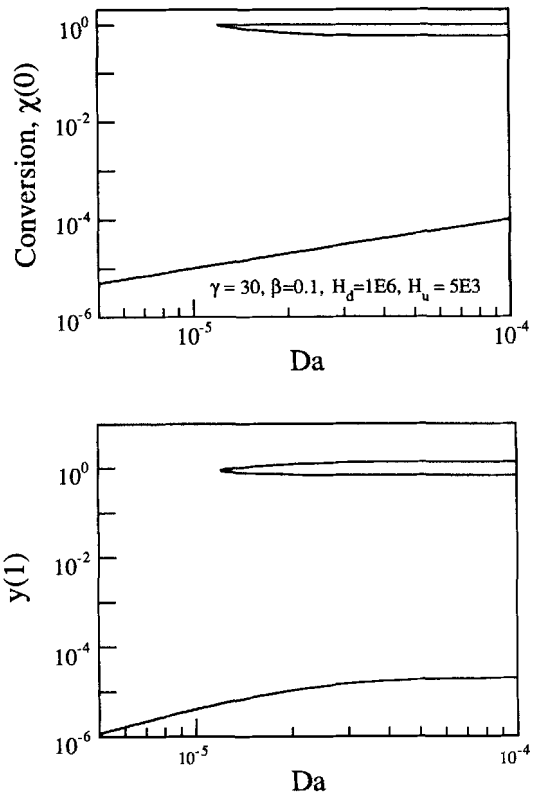

Figure 8. Bifurcation diagrams of bottom temperature and exit conversion vs. *Da* (residence time) for parameter values in region II.

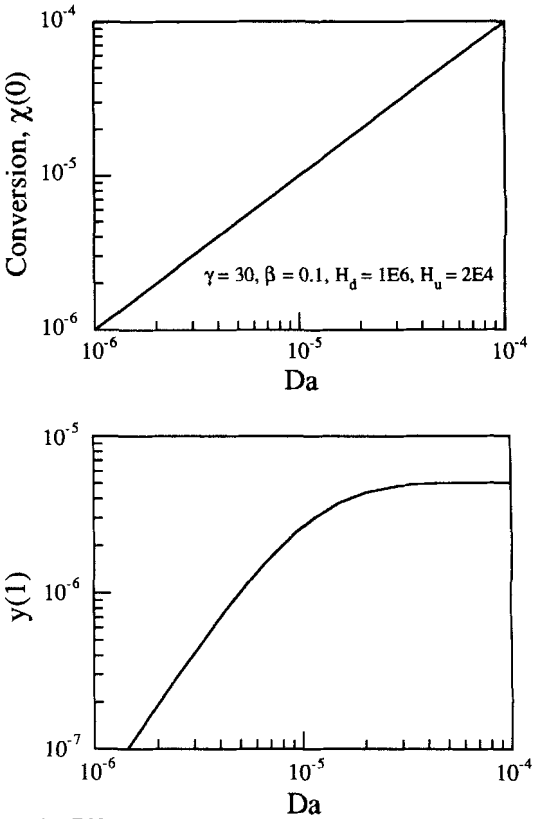

Figure 9. Bifurcation diagrams of bottom temperature and exit conversion vs. *Da* (residence time) for parameter values in region III.

For the nonadiabatic reactor, the uniqueness-multiplicity boundary consists of two segments. The first segment is defined by the hysteresis variety. The second segment is defined by the boundary limit variety, BLE. We note, however, that for typical parameter values the boundary limit variety BLE is the surface that defines the uniqueness-multiplicity boundary. By approximating the ignition and extinction points for the strongly cooled model, we can determine analytical criteria for predicting the boundary limit variety.

Determination of Ignition and Extinction Locus

In analyzing the bifurcation behavior of the nonadiabatic reactor, we observe that the ignition and extinction points are described for the most part by the limiting models of the adiabatic and strongly cooled case. In a previous work, we developed analytical expressions for predicting the ignition and extinction points of the adiabatic case. Here, we develop similar criteria for the prediction of the strongly cooled ignition and extinction locus which correspond to the boundary limit set (BLI and BLE).

We are interested in analyzing the bifurcation behavior for the case where the residence time is taken as the distinguished (bifurcation) parameter. We may construct the bifurcation sets in two different ways. The first method is the most straightforward and involves constructing the locus of ignition and extinction points in the $(H_u - Da)$ plane for a fixed value of H_d. In this case, varying the Damkohler number corresponds to changing the residence time. The second method involves fixing the ratio of α/St, or equivalently H_u/H_d, and projecting the locus of limit points in the $(St\text{-}Da)$ plane. In this case, following a line of constant slope H_d corresponds to increasing α and St at the same rate.

Figure 10 shows the bifurcation set for a fixed, γ, β and H_d projected in the $H_u - Da$ plane. For small values of H_u, the ignition and extinction loci correspond to essentially those of the adiabatic case. For higher values of H_u, we observe the two strongly cooled asymptotes where the ignition and extinction loci become independent of the Damkohler number.

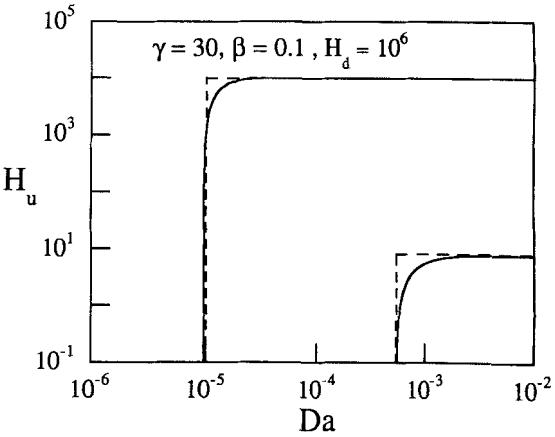

Figure 10. Cross-section of the bifurcation set in the (*St*, *Da*) plane for $\gamma = 30$, $\beta = 0.1$, $H_d = 10^6$.

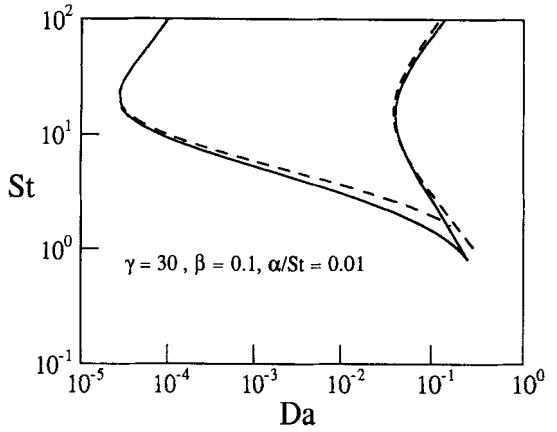

Figure 11. Cross-Section of the bifurcation set in the (*St*, *Da*) plane for $\gamma = 30$, $\beta = 0.1$, and $(H_d/H_d) = 0.01$.

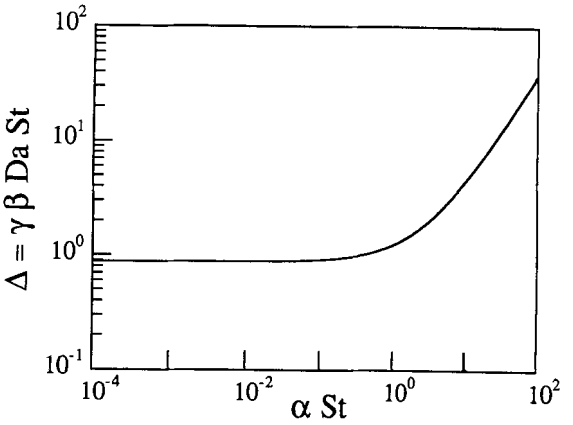

Figure 12. Dependence of Δ at the ignition point on αSt for the simplified model described by Eqs. 40-41.

Thus, the nonadiabatic case is described by four distinct asymptotes of the adiabatic ignition and extinction and the strongly-cooled ignition and extinction. The dashed lines indicating the four asymptotes correspond to the analytical predictions for the adiabatic and strongly cooled ignition and extinction points.

Figure 11 shows the bifurcation set for the nonadiabatic case for $\gamma = 30$, $\beta = 0.1$ and a fixed ratio of $\alpha/St = 0.01$. The dashed curves compare the approximations of the ignition and extinction locus which are derived in the next two sections. For this case, following lines of slope H_d corresponds to increasing or decreasing the residence time. Again, we note that the nonadiabatic case is essentially described by two limiting regimes of the adiabatic and strongly cooled case. In the region near the cusp point, at small values of the Stanton number the bifurcation set is close to that of the adiabatic case, while for high Stanton numbers the ignition and extinction curves turn and become straight lines. These asymptotes of slope H_d characterize the strongly cooled case. At the values of H_d, which characterize these asymptotes, the ignition and extinction points become independent of the Damkohler number. If one constructs various lines at different values of H_d, one will observe the ignition and extinction behavior corresponding to three types of bifurcation diagrams shown in Figures 7-9.

Determination of ignition points

To describe the ignition points, we return to Eqs. 6-8. Since we are interested in small values of β, we make the positive exponential approximation. For the determination of ignition points, we also neglect reactant consumption and obtain the following model:

$$\frac{d^2\theta}{d\xi^2} - \alpha \frac{d\theta}{d\xi} - \alpha\, St\, \theta + \gamma\beta St\, Da \exp\left\{\theta + \frac{1}{St}\frac{d\theta}{d\xi}\right\} = 0 \quad (38)$$

$$\theta(\xi = 0) = 0; \quad \frac{d\theta}{d\xi}(\xi = 1) = 0. \quad (39)$$

Again, we can simplify our analysis by eliminating parameters and considering only the case of practical interest. We assume that St is large and α is small. Therefore, we neglect the terms containing θ' in the exponent and in the differential equation. This results in the following model for the ignition locus:

$$\frac{d^2\theta}{d\xi^2} - \alpha\, St\, \theta + \gamma\beta\, St\, Da \exp(\theta) = 0 \quad (40)$$

$$\theta = 0; \quad \xi = 0$$

$$\frac{d\theta}{d\xi} = 0; \quad \xi = 1. \quad (41)$$

This model contains only two parameters, $\Delta = \gamma\beta\, Da\, St$ and αSt. The ignition locus can be described as a single curve in terms of these two parameters. Figure 12 shows the ignition locus in the (Δ, αSt) plane. We note that this model includes the adiabatic model ($\alpha = 0$) as a limiting case. In the limit that αSt is very small, the ignition locus is defined by the adiabatic case, which is described by the Frank-Kamenetskii thermal explosion model (Frank-Kamenetskii, 1969) that has a single ignition point at:

$$\Delta = \gamma\beta\, Da\, St = 0.8785 \quad (42)$$

$$\theta(1) = 1.187.$$

In the limit that αSt is large, the ignition locus is described by the strongly cooled model. The ignition point for the strongly cooled case results from ignoring the second derivative term (conduction term) and examining the resulting equation (for details, see Balakotaiah, 1989):

$$\frac{\Delta}{\alpha St} = \theta \exp(-\theta). \quad (43)$$

This equation has no solution when $(\Delta/\alpha St) > e^{-1}$. This limit of e^{-1} defines the ignition locus for large αSt. Substitution for Δ and α gives the following relationship for the strongly cooled ignition locus:

$$H_u = \gamma\beta e. \tag{44a}$$

In the case that the ratio of $\alpha/St =$ constant $= c$, the strongly cooled asymptote occurs along a line of constant slope:

$$H_d = \frac{\gamma\beta e}{c}. \tag{44b}$$

Determination of extinction points

We determine the extinction points for the nonadiabatic case in the same manner as for the adiabatic case. Again, we start with the model described by Eqs. 6-8. We assume that Stanton is large and $\alpha << St$ so that the terms containing $(dy/d\xi)$ can be dropped:

$$\frac{d^2y}{d\xi^2} - \alpha St\, y + \beta\, St\, Da\, (1-\chi) \exp\left\{\frac{\gamma y}{1+y}\right\} = 0 \tag{45}$$

$$\frac{d\chi}{d\xi} + Da\, (1-\chi) \exp\left\{\frac{\gamma y}{1+y}\right\} = 0 \tag{46}$$

$$\chi(\xi = 1) = 0;\ y(\xi = 0) = 0;\ \frac{dy}{d\xi}(\xi = 1) = 0. \tag{47}$$

We assume that the reaction occurs in only a very small region at the bottom of the reactor (point source) and that the reactor tubes act only as a heat exchanger. We drop the reaction term from Eq. 47 and replace the temperature continuity boundary condition at the bottom of the reactor with a source term boundary condition:

$$y(1) = y^*. \tag{48}$$

The solution of the linear differential equation results in the following expression for the temperature profile along the reactor:

$$y(\xi) = y^* \frac{\sinh \sqrt{\alpha St}\xi}{\sinh \sqrt{\alpha St}}. \tag{49}$$

By combining the species and energy balances and integrating, we obtain an expression relating the bottom temperature, y^* to the exit conversion χ_e:

$$y^* = \beta^* \chi_e, \tag{50}$$

where

$$\beta^* = \beta \sqrt{\frac{St}{\alpha}} \tanh \sqrt{\alpha St}. \tag{51}$$

The steady-state equation is obtained by integrating the species balance (Eq. 46):

$$F(\chi_e, \gamma, \beta^*, St, \alpha) = Da \frac{\tanh \sqrt{\alpha St}}{\sqrt{\alpha St}} - g(\chi_e, \gamma, \beta^*) \tag{52}$$

where

$$g(\chi_e, \gamma, \beta^*) = \frac{\gamma\beta^*\, \chi_e \ln\left(\frac{1}{1-\chi_e}\right) \exp\left\{\frac{-\gamma\beta^* \chi_e}{1+\beta^* \chi_e}\right\}}{(1+\beta^*\, \chi_e)^2}. \tag{53}$$

We note that Eqs. 52-53 describe the steady-state behavior on the ignited branch for both the adiabatic and strongly cooled limits. In the adiabatic limit,

$$\sqrt{\alpha St} << 1,\ \tanh \sqrt{\alpha St} \approx \sqrt{\alpha St}, \tag{54a}$$

and for the strongly cooled limit,

$$\sqrt{\alpha St} >> 1,\ \tanh \sqrt{\alpha St} \approx 1. \tag{54b}$$

If we substitute the expression given by Eq. 54a into Eqs. 51-53, the equations reduce to that for the adiabatic case as considered previously and the extinction locus can be written in a parametric form (Lovo and Balakotaiah, 1991). If we substitute the relation given by Eq. 54b into the steady-state equation, we can also derive the extinction boundary limit set in a parametric form. In this case the maximum possible bottom temperature rise is given by Eq. (50) with:

$$\beta^* = \beta \sqrt{\frac{St}{\alpha}}. \tag{55}$$

In the strongly cooled limit, the extinction locus becomes independent of the Damkohler number. It can be described in the following parametric form:

$$\beta^* = G(\chi_e, \gamma) \quad (0 < \chi_e < \chi_e^*) \tag{56a}$$

$$D = \frac{1}{\sqrt{H_d\, H_u}} = g(\chi_e, \gamma, \beta^*). \tag{56b}$$

The function $g(\chi_e, \gamma, \beta^*)$ is given by Eq. 53, and $G(\chi_e, \gamma)$ is defined as:

$$G(\chi_e, \gamma) = \frac{B(\chi_e) \pm \sqrt{B(\chi_e)^2 - 4\, C(\chi_e)}}{2\, \chi_e C(\chi_e)} \tag{57a}$$

$$A(\chi_e) = 1 + \frac{\chi_e}{(1-\chi_e) \ln\left(\frac{1}{1-\chi_e}\right)} \tag{57b}$$

$$B(\chi_e) = \frac{\gamma+2}{A(\chi_e)} - 2 \tag{57c}$$

$$C(\chi_e) = 1 - \frac{2}{A(\chi_e)} \tag{57d}$$

where χ_e^* is defined by:

$$B(\chi_e^*)^2 - 4\, C(\chi_e^*) = 0. \tag{57e}$$

The dashed lines marked on Figure 10 correspond to the adiabatic and strongly cooled extinction asymptotes using these approximations and are in excellent agreement with the numerically computed asymptotes for the full model.

For the special case of the Stanton formulation, we can express the entire extinction locus in the following parametric form:

$$\beta^* = G(\chi_e, \gamma) \tag{58a}$$

$$\sqrt{\alpha St} = \tanh^{-1}\left(\frac{\beta^*}{\beta}\sqrt{\frac{\alpha}{St}}\right) \tag{58b}$$

$$Da = \frac{\sqrt{\alpha St}}{\tanh\sqrt{\alpha St}}\, g(\chi_e, \gamma, \beta^*). \tag{58c}$$

The dashed curve marked on Figure 11 corresponds to the approximate extinction locus determined by Eq. 58 and is in excellent agreement with the numerical results of the full model, with the exception of the region near the cusp point. For the residence time formulation, we are able to express only the adiabatic and strongly cooled limits analytically. However, the extinction points of the steady-state equation defined by Eqs. 51-53 describe the entire extinction locus very accurately.

For typical values of H_d ($10^5 - 10^8$), the boundary between autothermal and nonautothermal operation can be defined by the single criterion of the boundary limit set (BLE). For cases of practical interest, the analytical criterion given by Eqs. 56a and 56b provides an excellent approximation of this boundary. In addition to providing an analytical criterion, this expression reduces the number of parameters (since β^* enters as $\beta\sqrt{(H_d/H_u)}$. Thus, instead of constructing the autothermal boundary for each γ (activation energy) and β (heat of reaction or concentration) of interest, as in Figure 6, we construct the boundary for each activation energy of interest. Figure 13 shows the boundaries between autothermal operation and nonautothermal operation for typical values of the activation energy using Eq. 56.

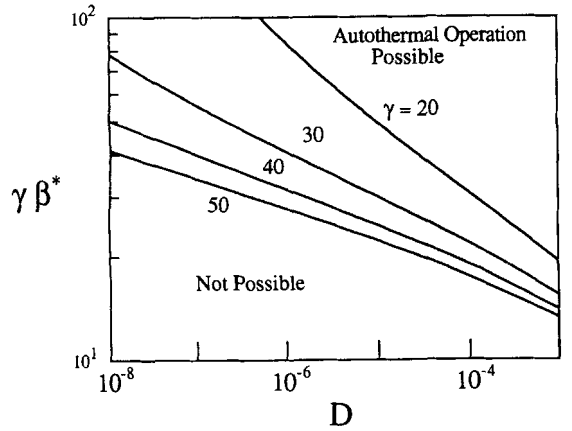

Figure 13. Boundary between autothermal and nonautothermal operation for some typical γ values.

Practical Criteria for Autothermal Operation

We also develop analytical expressions for the boundary between autothermal and nonautothermal operation using the reaction temperature as a reference. As in the adiabatic case, this often provides a more practical criterion since it is usually the case that the reaction temperature is specified. In addition, the reaction rate is usually measured at this temperature. We rewrite the steady-state equation for the strongly cooled case using the following substitutions:

$$T_R = T_0 + \Delta T_{ad}\sqrt{\frac{U_d d_d}{U_u d_u}} \tag{59}$$

$$\gamma = \frac{E}{RT_0} = \frac{E}{RT_R}\frac{T_R}{T_0} = \gamma_R y_R \qquad \beta^* = \frac{\Delta T_{ad}}{T_0}\sqrt{\frac{U_d d_d}{U_u d_u}} = \beta_R^* y_R$$

$$y_R = \frac{T_R}{T_0} \qquad \beta_R^* = \frac{\Delta T_{ad}}{T_R}\sqrt{\frac{U_d d_d}{U_u d_u}}$$

$$H_{dR} = \frac{U_d A_{hd}}{\rho_f C_{pf} k(T_R)\, V_r} \qquad H_{uR} = \frac{U_u A_{hu}}{\rho_f C_{pf} k(T_R)\, V_r}$$

$$B_R^* = \gamma_R \beta_R^* = \left(\frac{E}{RT_R}\right)\left(\frac{\Delta T_{ad}}{T_R}\right)\sqrt{\frac{U_d d_d}{U_u d_u}}.$$

Here, $(T_R - T_0)$ is the maximum possible preheating of the reaction mixture. On the ignited branch where the conversion is close to unity, the bottom (reaction) temperature is approximately equal to T_R. Here, γ_R and β_R^* are the dimensionless activation energy and dimensionless preheating parameter, respectively. Substitution of Eq. 59 into Eqs. 53 and 56 gives:

$$D_R = \frac{1}{\sqrt{H_{dR}H_{uR}}} = \frac{\gamma_R \beta_R^* \chi_e}{[1-\beta_R^*(1-\chi_e)]^2}\exp\left\{\frac{\gamma_R\,\beta_R^*\,(1-\chi_e)}{1-\beta_R^*(1-\chi_e)}\right\}\ln\left(\frac{1}{1-\chi_e}\right). \tag{60}$$

The following equation gives the relationship between the feed temperature and the bottom (reaction) temperature as a function of β_R^* and χ_e:

$$\frac{T_0}{T_R} = 1 - \beta_R^* + \beta_R^*\,(1-\chi_e). \tag{61}$$

Figure 14 shows boundaries between autothermal and nonautothermal operation predicted by the extinction points of Eq. 60. If both (D_R, β_R^*) and $[(T_0/T_R), \beta_R^*]$ fall in the region of autothermal operation, then an ignited steady state exists for residence times exceeding some critical value. When the parameters fall exactly on the boundary, the extinction point is at infinite residence times. When the parameters are in the region of autothermal operation but close to the boundary, the critical residence time can be found from Eq. 58. Further from the boundary, the critical residence time moves to and stabilizes at the adiabatic values.

We note that the curves for γ_R = 20, 30, and 40 in Figure

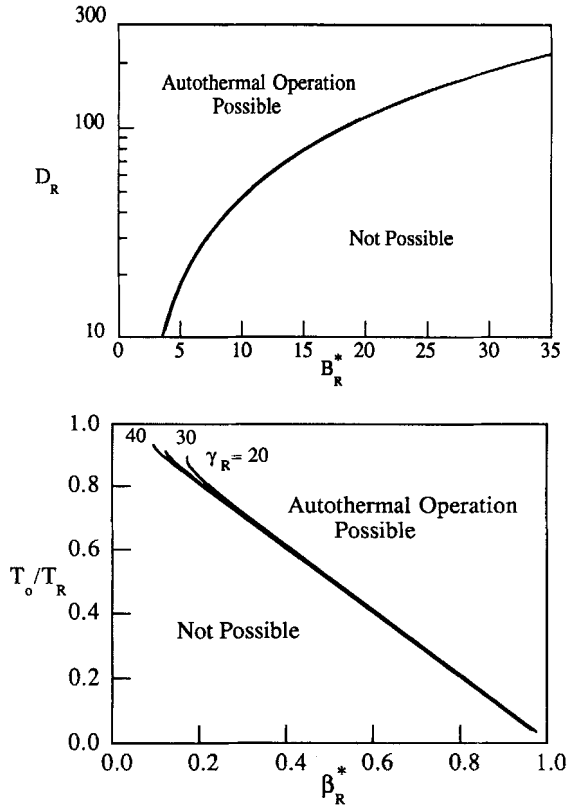

Figure 14. Boundaries of the region of autothermal operation in terms of the reaction temperature.

14 are nearly coincident and that the boundary of the region of autothermal operation can be described by a single curve. A simple criterion for autothermal operation can be developed by simplifying Eq. 60 making use of large activation energy asymptotics and finding the extinction point. The criterion may be written in the following parametric form:

$$D_R = \frac{1}{\sqrt{H_{dR} H_{uR}}} = \frac{\rho_f C_{pf}\, k(T_R)\, V_r}{\sqrt{U_d\, U_u\, A_{hd}\, A_{hu}}} = \exp\left(v + \frac{1}{v}\right) \qquad (62a)$$

$$B_R^* = \gamma_R\, \beta_R^* = v \exp\left(\frac{1}{v}\right) \text{ for } 0 < v < 1, \qquad (62b)$$

where

$$v = B_R^*(1 - \chi_e). \qquad (62c)$$

These approximations make use of the fact that conversions are close to unity (for details, see Lovo and Balakotaiah, 1991). Therefore, we can approximate Eq. 61 as:

$$\frac{T_0}{T_R} = 1 - \beta_R^*. \qquad (63)$$

Equation 63 gives the relation between the feed and reaction temperature, while Eq. 62 may be used to determine the critical heat loss at which the ignited branch disappears.

Conclusions and Remarks

The steady-state behavior of the nonadiabatic, autothermal reactor with internal countercurrent heat exchange was analyzed comprehensively. The multiplicity features of the nonadiabatic model are characterized by the two limiting cases of the adiabatic and strongly cooled models. In a previous work, we have characterized the multiplicity features of the adiabatic case. Here, we examined the multiplicity features of the nonadiabatic case and developed analytical expressions for the uniqueness-multiplicity boundary and ignition and extinction points for the strongly cooled case.

Important results include determining whether or not autothermal operation is possible and what residence times are needed to achieve autothermal operation. It is found that at a critical value of heat loss parameter H_u, the extinction point moves to infinite residence times. Beyond this point, an ignited steady state no longer exists. Thus, the extinction boundary limit set defines the boundary between autothermal and nonautothermal operation. This important result is summarized in Figures 13 and 14. The analytical expressions given by Eqs. 62–63 accurately describe the boundaries shown in Figure 14.

We have restricted our analysis to the case of first-order reactions. However, the same approach can be used to develop analogous criteria for autothermal operation for other types of kinetic expressions (nth-order reactions) as well as reversible reactions. The systematic approach taken here can also be extended to other nonadiabatic reactor models.

Acknowledgment

This research is supported by the Gulf Coast Hazardous Substances Research Center, (GCHSRC), the American Chemical Society Petroleum Research Fund, and the Robert A. Welch Foundation.

Notation

A_h = heat exchange area
B = dimensionless parameter $= \frac{E}{RT_0}\frac{\Delta T_{ad}}{T_0}$
B^* = dimensionless parameter $= \frac{E}{RT_0}\frac{\Delta T_{ad}}{T_0}\frac{UA_h}{q\rho_f C_{pf}}$
B_R^* = dimensionless parameter, $\gamma\beta_R^*$
C_A = concentration of species A
C_{pf} = heat capacity per unit mass of fluid
D = Dimensionless parameter $= \frac{1}{\sqrt{H_d H_u}}$
Da = Damkohler number at inlet conditions $= \frac{k(T_0)V_r}{q}$
Da_R = Damkohler number at reaction conditions $\frac{k(T_R)V_r}{q}$
E = activation energy
H = dimensionless overall heat transfer coefficient, defined by Eq. 37
$(-\Delta H_r)$ = heat of reaction
k = first order reaction rate constant
q = volumetric flow rate
R = universal gas constant
St = Stanton number for heat transfer between tubes
T = absolute temperature

ΔT_{ad} = adiabatic temperature rise $= \dfrac{(-\Delta H_r)C_{A0}}{\rho_f C_{pf}}$

U = overall heat transfer coefficient

V_r = reactor volume

x = axial distance along reactor

y = dimensionless temperature

Greek letters

α = Stanton number for heat loss to surroundings $= \dfrac{A_{hu}U_u}{q\,\rho_f C_{pf}}$

β = dimensionless adiabatic temperature rise

β^* = maximum possible preheating parameter, Eq. 51

β_R^* = maximum possible preheating parameter based on reaction conditions

δ = dimensionless parameter, Eq. 20

Δ = Frank-Kamenetskii number, Eq. 42

η = scaled axial coordinate, Eq. 25

χ = conversion of species A

γ = dimensionless activation energy, E/RT_o

γ_R = dimensionless activation energy (reaction), E/RT_R

ρ = density

θ = dimensionless temperature, $\gamma\, y$

ξ = dimensionless distance along reactor

Subscripts

d = downtube

f = fluid

o = inlet conditions

R = reaction conditions

u = uptube

Literature Cited

Adomaitis, R., and A. Cinar, "The Bifurcation Behavior of an Autothermal Packed Bed Tubular Reactor," *Chem. Eng. Sci.*, **43**, 887 (1988).

Ampaya, J., and R. G. Rinker, "Design Correlations for Autothermal Reactors with Internal Countercurrent Heat Exchange," *Ind. Eng. Chem. Process Des. Dev.*, **16**, 63 (1977).

Ampaya, J., and R. G. Rinker, "Autothermal Reactors with Internal Heat Exchange: I," *Chem. Eng. Sci.*, **32**, 1327 (1977).

Baddour, R., P. Brian, B. Logeais, and J. Eymery, "Steady-State Simulation of an Ammonia Synthesis Converter," *Chem. Eng. Sci.*, **20**, 281 (1965).

Balakotaiah, V., and D. Luss, "Global Analysis of the Multiplicity Features of Multi-Reaction Lumped-Parameter Systems," *Chem. Eng. Sci.*, **39**, 865 (1984).

Balakotaiah, V., "Simple Runaway Criteria for Cooled Reactors," *AIChE J.*, **35**, 1039 (1989).

Frank-Kamenetskii, D. A., *Diffusion and Heat Transfer in Chemical Kinetics*, Plenum Press, New York (1969).

Inoue, H., and T. Komiya, "On the Stability of Autothermal Reactors," *Int. Chem. Eng.*, **8**, 749 (1968).

Kaufmann, L. A., and H. Peterschek, "Modeling Vertech's Mile Long Reactor," *Chem. Eng. Sci.*, **41**, 685 (1986).

Lovo, M., H. A. Deans, and V. Balakotaiah, "Modeling and Simulation of Aqueous Hazardous Waste Oxidation in Deep Well Reactors," *Chem. Eng. Sci.*, **45**, 2703 (1990).

Lovo, M., and V. Balakotaiah, "Multiplicity Features of Adiabatic Autothermal Reactors," *AIChE J.*, **38**, 101 (1992).

Lovo, M., "Steady-State and Transient Behavior of a Deep Well Oxidation Reactor," PhD Thesis, Univ. of Houston (1991).

Van Heerden, C., "Autothermic Processes: Properties and Reactor Design," *Ind. Eng. Chem.*, **45**, 1242 (1953).

Van Heerden, C., "The Character of the Stationary State of Exothermic Processes," *Chem. Eng. Sci.*, **8**, 133 (1958).

Witmer, G. S., V. Balakotaiah, and D. Luss, "Finding Singular Points of Two-Point Boundary Value Problems," *J. Comp. Phys.*, **65**, 244 (1986).

Manuscript received Apr. 22, 1991, and revision received Nov. 18, 1991.